Synergistic effects of hydrogenation and a noble metal on the topotactic and magnetic modulations of manganite films

Chuanwei Huang(黄传威)[1], Yonggang Xia(夏永刚)[1], Haiping Zhou(周海平)[2], Yukuai Liu(刘愉快)[3,†], and Jiahui Ou(区嘉辉)[1,‡]

[1] *Shenzhen Key Laboratory of Special Functional Materials, Guangdong Provincial Key Laboratory of New Energy Materials Service Safety, College of Materials Science and Engineering, Shenzhen University, Shenzhen* 518060, *China*

[2] *School of Materials and Energy, University of Electronic Science and Technology of China, Chengdu* 611731, *China*

[3] *College of Electronic Information and Mechatronic Engineering, Zhaoqing University, Zhaoqing* 526061, *China*

(Received 6 September 2025; revised manuscript received 7 November 2025; accepted manuscript online 11 November 2025)

The search for high-temperature ferromagnetic insulators is crucially important for low-power spintronic storage devices. However, very few ferromagnetic insulating materials with a Curie temperature above 300 K have been reported to date, which greatly hinders their practical applications. Here, using a hydrogen plasma reduction method, we modulated the topotactic structure, resultant magnetism, and electrical insulation in $La_{0.7}Sr_{0.3}MnO_3$ films constrained by different misfit strains. We observed an ultrafast structural transformation from the pristine $La_{0.7}Sr_{0.3}MnO_3$ perovskite state to the hydrogenated brownmillerite $La_{0.7}Sr_{0.3}MnO_{2.5}$ state as a function of the bias voltage of a low-frequency inductively coupled plasma system. Meanwhile, Pt electrodes capped on the film surfaces further promote the stabilization of the hydrogenated brownmillerite $La_{0.7}Sr_{0.3}MnO_{2.5}$, accompanied by enhanced magnetic insulation for temperatures up to 400 K. Such subtle engineering of functional perovskite-derived oxide films offers insights into the development of emergent materials for promising spin-polarized tunneling devices.

Keywords: perovskite–brownmillerite transition, pulsed laser deposition, hydrogen plasma treatment, manganite films, magnetic insulator

PACS: 77.80.B–, 64.60.–i, 81.15.Fg, 52.40.Hf, 52.40.Hf, 75.50.–y

DOI: 10.1088/1674-1056/ae1dea **CSTR:** 32038.14.CPB.ae1dea

The ever-growing need for high data processing speeds and large data storage capabilities has caused a significant increase in energy consumption and environmental concerns, driven by massive digital data generation.[1,2] New-generation quantum electronic devices that utilize the spin-polarized tunneling effect offer great potential in this regard, making them outstanding candidates for energy-efficient and large-scale data storage and processing.[3] In this context, one of the notable features of these devices is the use of highly spin-polarized electron tunneling through ferromagnetic insulating materials (FMIs). Notwithstanding unceasing progress in the development of various FMIs,[4–9] very few FMIs with a high Curie temperature (T_C) have been reported for operational temperatures above 300 K.[10–13] These obstacles have largely prevented the application of FMIs in practical spintronic devices.

Perovskite oxides are prime candidates for spin filters as they simultaneously exhibit high spin polarization and electrical insulation, positioning them as front-runners for ultra-low-power spintronic devices and energy-efficient memory and logic applications. In particular, manganites ($La_xSr_{1-x}MnO_3$) have attracted extensive attention due to their emergent physical properties ranging from ferromagnetism, metal–insulator transition (MIT) and colossal magnetoresistance, achievable through composition and interfacial strain engineering.[14–17] Although $La_{0.7}Sr_{0.3}MnO_3$ with a high T_C ($\sim$ 370 K) is a promising material for spintronic devices, interfacial strain has been shown to substantially reduce T_C and ferromagnetism.[16,18] Meanwhile, traditional cation substitution strategies fail to simultaneously optimize magnetic ordering and insulating resistivity.[19] Moreover, oxygen-deficiency-sensitive perovskite oxides usually undergo distortions in their crystal and electronic structures, contributing to severely degraded T_C and spin polarization.[16,20] These degradations mainly stem from oxygen-vacancy-mediated suppression of the Mn^{3+}/Mn^{4+} ratio, which concomitantly quenches the double-exchange interaction essential for desirable ferromagnetic properties.

Recently, topochemical engineering via anionic oxygen (O^{2-}) has provided pathways to attain novel structures and electronic properties in perovskite-derived oxide films.[21–25] Hydrogenation in particular has emerged as a facile route, triggering distinct B–O coordination geometries and topotactic phases while modulating diverse electronic properties such as superconductivity, MIT, and FMI.[23,26,27] Notably, ultrafast hydrogen plasma treatment of perovskite oxide films in-

†Corresponding author. E-mail: liuyukuai@zqu.edu.cn

‡Corresponding author. E-mail: 2019201030@email.szu.edu.cn

© 2026 Chinese Physical Society and IOP Publishing Ltd. All rights, including for text and data mining, AI training, and similar technologies, are reserved.

CPB Online In-Press

duces a series of topotactic phase transitions from perovskite (PV-ABO_3) to brownmillerite (BM-$ABO_{2.5}$).[17] Such a transformation enables precise modulation of the valence states of the transition metal ion, coordination frameworks, and oxygen vacancy channels, as well as the concomitant magnetic exchange interaction and electrical resistivity. Enormous progress has been made in realizing perovskite-derived oxide materials with various topotactic phases and functionalities. Nevertheless, the discovery of new FMI materials exhibiting magnetic insulation above room temperature remains critical for practical applications.[26,28]

Previous studies reported that subtle modulation of coordination geometries (such as arrangements of BO_6 and BO_4 polyhedra) within the BM phase via hydrogenation intercalation facilitates emergent physical properties.[25,29] Here, we deployed hydrogen plasma technology to treat the PV-LSMO(7/3) films constrained with interfacial strains (Figs. 1(a) and 1(b)). The hydrogen plasma, possessing high kinetic energy and strong chemical reactivity, not only enhances overall efficiency but also facilitates the reduction of manganese oxides, ultimately forming oxygen-deficient $La_{0.7}Sr_{0.3}MnO_{3-\delta}$ [LSMO(7/3), $0.0 \leq \delta \leq 0.5$] oxides. An optimized hydrogenation bias voltage (~ -180 V) resulted in a topotactic transition from PV-$La_{0.7}Sr_{0.3}MnO_3$ to BM-$La_{0.7}Sr_{0.3}MnO_{2.5}$ in constrained LSMO(7/3) films, accompanied by a change from a ferromagnetic metallic state to an antiferromagnetic insulating one. In contrast, only an oxygen-deficient PV phase formed in the unconstrained LSMO(7/3)/$LaSrGaO_4$ (LSGO) system. Furthermore, electrodes capped with the noble metal Pt deposited on the LSMO(7/3) surface accelerated the topotactic transformation, yielding a weak magnetic insulating state ($T_C > 400$ K) in the BM phase (Fig. 1(c)). Thus, these synergistic effects establish a paradigm for achieving high-temperature FMI states in perovskite-derived oxides, advancing the potential for spintronic integration. This work is further distinguished by the occurrence of ferromagnetic insulation above room temperature.

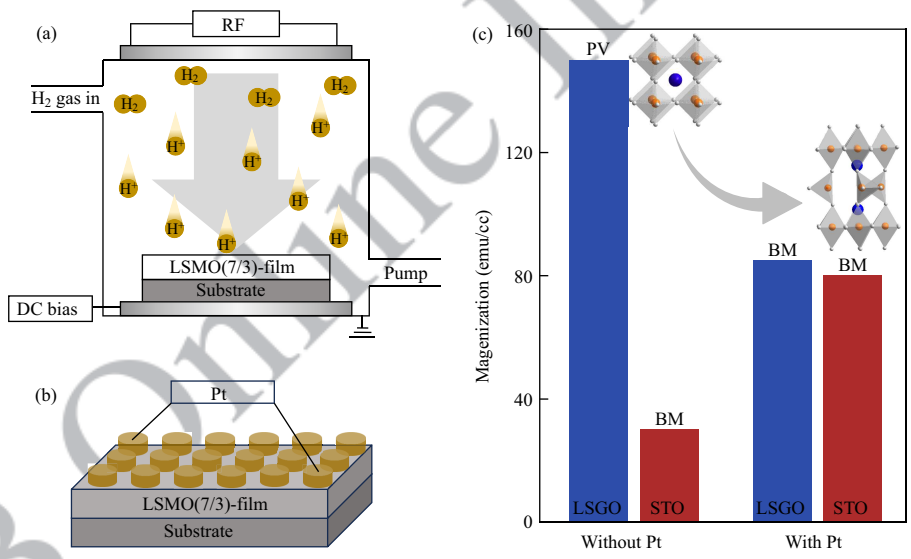


Fig. 1. (a) Schematic of hydrogen plasma intercalation into LSMO(7/3) films. (b) Illustration of epitaxial LSMO(7/3) film with Pt electrodes. (c) Structure evolution from PV to BM and corresponding magnetic properties.

LSMO(7/3) films with a thickness of 20 nm were epitaxially deposited on (001)-oriented $SrTiO_3$ (STO) and $LaSrGaO_4$ (LSGO) single-crystal substrates via pulsed laser deposition employing a KrF excimer laser ($\lambda = 248$ nm) at 1.6 J/cm^2 fluence. During growth, the substrates were held at 700 °C under an oxygen partial pressure of 30 Pa with the target-to-substrate distance fixed at 3.0 cm. Top electrodes (Pt, 50 μm×50 μm) were fabricated by magnetron sputtering.

Postdeposition cooling to room temperature proceeded at 15 °C/min in the deposition atmosphere. Subsequently, these films underwent hydrogen plasma treatment for 10 min at 30 °C using a low-frequency inductively coupled plasma system (Fig. 1(a)) with parameters set to 1800 W discharge power, 20 sccm H_2 flux and bias voltages of -80 V or -180 V. The negative voltage selectively facilitated hydrogen cation (H^+) injection — rather than H^- species or electrons — into the LSMO lattice to drive phase transformation.

Crystalline structures of different LSMO(7/3)/STO heterostructures were characterized by high-resolution four-circle x-ray diffraction (XRD, Rigaku Smart Lab). The magnetic properties of pristine and treated LSMO(7/3) films were measured using a superconducting quantum interference device magnetometer integrated within a magnetic property measurement system (PPMS, Quantum Design) across a temperature range of 10–400 K. Magnetothermal curves (M–T) were acquired at $H = 500$ Oe for LSMO(7/3) films with different phases.

We found that the facile hydrogen plasma treatment leads

CPB Online In-Press

to a phase transition in LSMO(7/3)/STO heterostructures, accompanied by interesting magnetic reconfigurations. XRD results (Fig. 2(a)) demonstrated that the pristine PV-LSMO(7/3) films exhibit a characteristic peak at $2\theta \approx 47.2°$. Meanwhile, robust ferromagnetism was evidenced by the saturated magnetizations of 500 emu/cm^3 measured at 10 K and 250 emu/cm^3 at 300 K, respectively (Figs. 2(b) and 2(c)). Thermal stability with $T_C \sim 350$ K was verified via a vibrating sample magnetometer (Fig. 2(d)).[30] Hydrogenation at a mild bias voltage (-80 V) initiates the transition of PV ($La_{0.7}Sr_{0.3}MnO_3$) to BM ($La_{0.7}Sr_{0.3}MnO_{2.5}$), shifting the (002) diffraction angle of PV from $\sim 47.2°$ to $\sim 43.8°$, which is the (008) diffraction angle of BM. Additionally, M_s is drastically suppressed to ~ 25 emu/cm^3 at 10 K (Figs. 2(b) and 2(c) inset), with T_C decreasing to ~ 300 K (Fig. 2(d) inset). Furthermore, a pure hydrogenated BM phase (HBM) occurs with a characteristic (006) angle of $\sim 32.6°$ in LSMO(7/3) films treated with a large voltage of ~ -180 V, resulting in an elongated c lattice (4.18 Å), compared with that of the conventional BM phase (4.11 Å).[31] Remarkably, this HBM phase retains weak magnetism, exhibiting an enhanced M_s of ~ 20 emu/cm^3 at 300 K (inset in Figs. 2(c) and 2(d)). This sharply contrasts with the antiferromagnetism of BM-LSMO(7/3) achieved via a conventional post-annealing process.[31] The distinct magnetism between the post-annealing-induced BM phase and the present HBM-LSMO(7/3) one may originate from additional implantation of H^+ in the hydrogenated LSMO(7/3) films. This magnetic difference implies that the significant H^+ incorporation gives rise to the topotactic phase transformation and the consequent variable manganese valence state, leading to high-temperature weak magnetism in the hydrogenated BM phase of LSMO(7/3) films. Concomitantly, the hydrogen plasma treatment induces a metal-to-insulator transition in the LSMO(7/3)/STO heterostructure. Compared with the metallic state observed in the pristine PV-LSMO(7/3) films, the HBM-LSMO(7/3) phase exhibits electrical insulation with the resistivity exceeding the limits of the PPMS.

Misfit strain imparted by the substrate also influences the hydrogen-induced topotactic transformations in different LSMO(7/3) heterostructures, as unambiguously evidenced by XRD and magnetic characterizations (Fig. 3). It is well known that tensile misfit strain significantly lowers the oxygen vacancy formation energy in oxide films whereas compressive strain plays a minor role.[32] To control the interfacial strain state, (001)-oriented single-crystal STO and LSGO substrates were selected, imposing misfit strains of $+0.06\%$ and -1.54% relative to bulk PV-LSMO(7/3), respectively. We speculate that tensile strain is conducive to oxygen migration and subsequent topotactic transformation in constrained LSMO(7/3) films. Accordingly, even an applied voltage of -180 V gives rise to an oxygen-deficient PV phase (i.e., $2\theta \sim 45.8°$) for the LSMO(7/3)/LSGO heterostructure system compared with the HBM phase observed in the tensile-strained LSMO(7/3)/STO system with a misfit strain of $\sim 1.54\%$ (Fig. 3(a)).

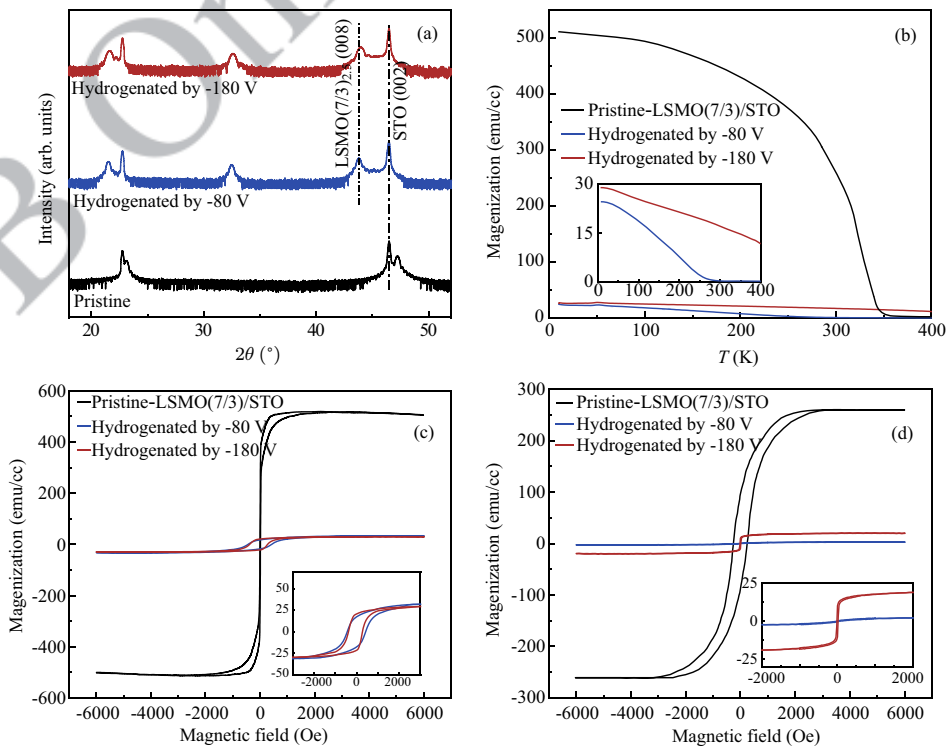


Fig. 2. Effect of bias voltage on LSMO(7/3)/STO films. (a) XRD patterns of pristine PV-LSMO(7/3) and hydrogenated BM-LSMO(7/3) with different voltage biases (i.e., -80 V and -180 V). (b) M–T curves from 10 K to 400 K for pristine and HBM-LSMO(7/3) films. (c), (d) Corresponding hysteresis loops measured at 10 K and 300 K.

CPB Online IP-Press

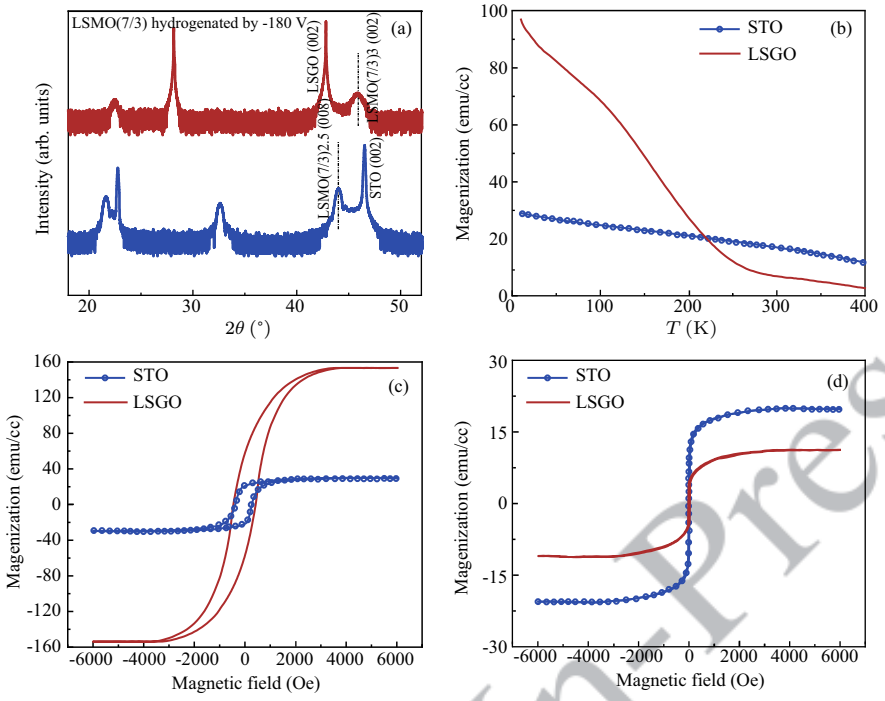


Fig. 3. Effect of misfit strain on hydrogen-treated LSMO(7/3) film grown on STO and LSGO substrates, respectively. (a) θ–2θ XRD scans of LSMO(7/3) films hydrogen-treated at −180 V. (b) M–T curves from 10 K to 400 K for hydrogenated LSMO(7/3)/STO and LSMO(7/3)/LSGO systems. (c), (d) Corresponding hysteresis loops measured at 10 K and 300 K, respectively.

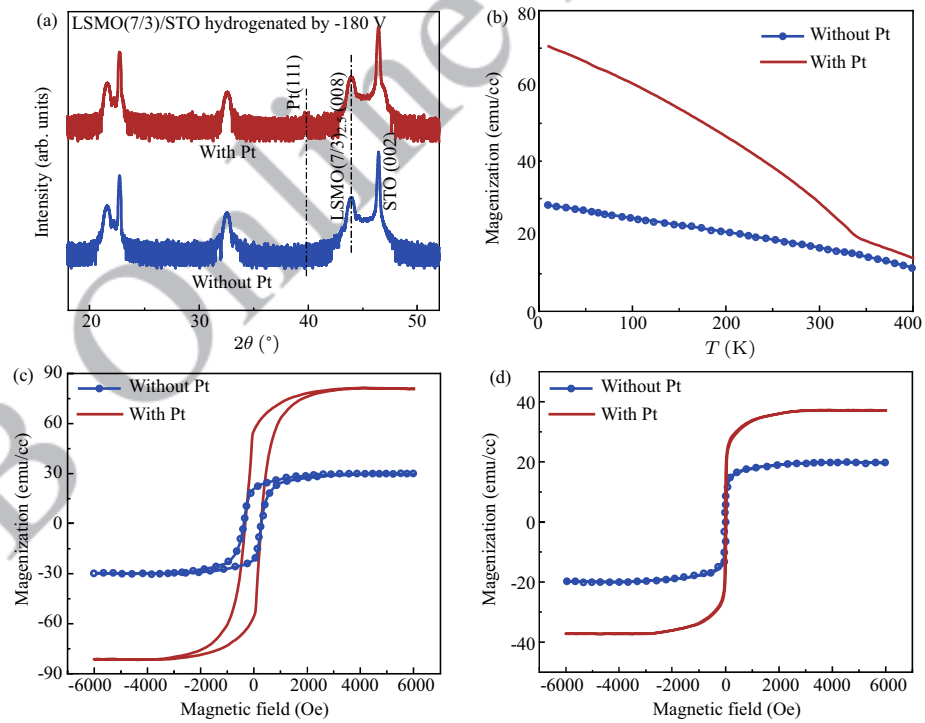


Fig. 4. Enhanced magnetic properties of tensile-strained HBM-LSMO(7/3)/STO through Pt capping. (a) XRD pattern of the hydrogenated LSMO(7/3)/STO system with (gray) and without (yellow) Pt capped electrodes. (b)–(d) M–T curves and hysteresis loops for the corresponding LSMO(7/3) films measured at 10 K and 300 K, respectively.

This strain-driven transformation concurrently alters the magnetic properties of hydrogenated LSMO(7/3) films. The M–T curves (Fig. 3(b)) demonstrate significantly suppressed magnetism at temperatures of < 250 K for the LSMO(7/3)/LSGO system, starkly contrasting with that of the compressively strained LSMO(7/3) film. The M–H loops of the hydrogenated LSMO(7/3)/LSGO system measured at 300 K (Figs. 3(c) and 3(d)) also show a weak magnetic signal with a negligible $M_s \sim 10$ emu/cm^3, consistent with the trend reported in oxygen-deficient LSMO(7/3) film.[33]

As established above, the PV–HBM transition is relatively difficult in bulk-like LSMO(7/3) compared with the film clamped by tensile strains. To tackle this challenge, a noble metal was employed to accelerate hydrogenation-

CPB Online In Press

induced topotactic transformation in manganite film.[34] Top electrodes (Pt, 50 μm×50 μm) were deposited to further attain differential structural and physical properties of LSMO(7/3) films (Fig. 4). XRD (Fig. 4(a)) shows insignificant structural differences in the hydrogenated BM-LSMO(7/3)/STO system with or without Pt electrodes, confirming complete PV–BM transition. A visible diffraction peak near $2\theta \approx 39.8^\circ$ corresponds to the (111)-oriented Pt electrode. Notably, magnetic properties undergo striking enhancements for the Pt/LSMO(7/3)/STO heterostructure. The M–T curve (Fig. 4(b)) implies a superior magneto-thermal stability in Pt-capped HBM-LSMO(7/3)/STO systems, sustaining an improved magnetic order at temperatures above 400 K. At 300 K (Fig. 4(d)), Pt-capped HBM-LSMO(7/3) exhibits a saturated magnetization (M_s) of 40 emu/cm^3. Thus, additional Pt electrodes enhance the magnetic robustness of tensile-strained HBM-LSMO(7/3) films.

However, the situation in LSMO(7/3)/LSGO systems exhibits distinct behavior, as shown in Fig. 5. After a similar hydrogenation, the Pt-capped PV-LSMO(7/3) film completely changed to a pure HBM phase with a characteristic diffraction peak at $\sim 43.8^\circ$, whereas the Pt-free LSMO(7/3) film retained an oxygen-deficient PV phase. Meanwhile, the Pt-capped HBM-LSMO(7/3) maintained magnetic ordering at temperatures above 400 K (gray curve in Fig. 5(b)), aligning with the HBM-LSMO(7/3)/STO system. Accordingly, the observed results substantiate that the capped Pt electrodes not only facilitate the topochemical reduction of the PV-LSMO(7/3) film but also result in further lattice distortion[35] and Mn–O hybridization[36] in the reduced BM-LSMO(7/3) films via consecutive H^+ intercalation. Therefore, the emergence of weak ferromagnetism in the hydrogenated HBM-LSMO(7/3) film can be attributed to the synergistic effects of H^+ implantation, interfacial strain and the Pt electrodes compared with the typical antiferromagnetism of the ideal BM phase in oxide films.[5,26,34]

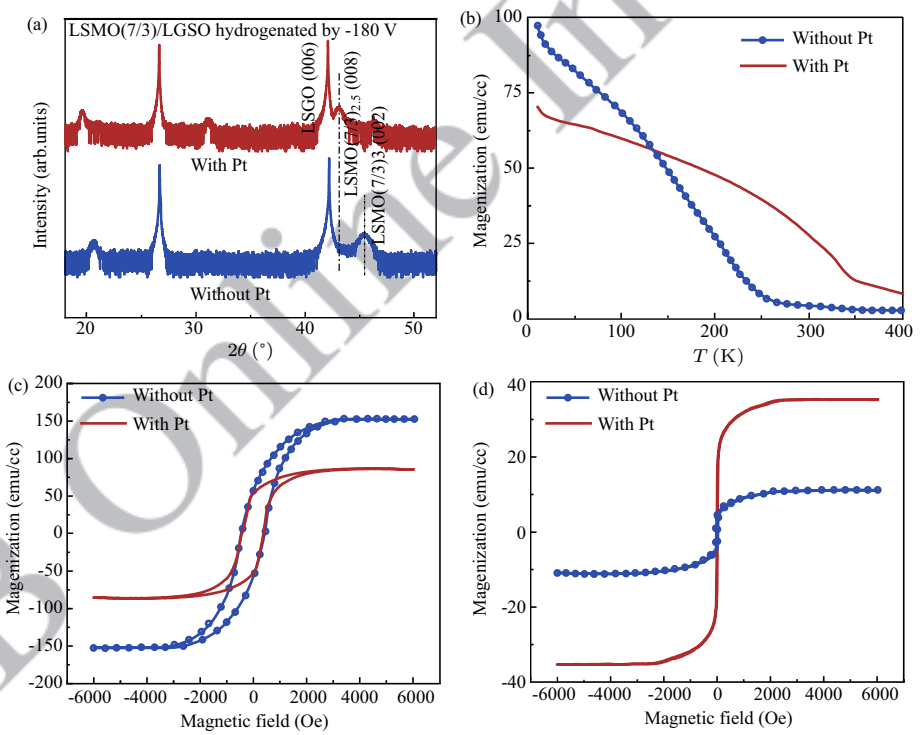


Fig. 5. Pt-induced phase transition in hydrogenated LSMO(7/3)/LSGO. (a) θ–2θ XRD scans for the hydrogenated LSMO(7/3) film deposited on LSGO, treated with (grey) or without (yellow) Pt electrodes. (b)–(d) Corresponding M–T and hysteresis loops of the hydrogenated LSMO(7/3) film measured at 10 K and 300 K, respectively.

In summary, we have demonstrated that a facile hydrogenation plasma treatment could quickly achieve a BM phase in LSMO(7/3) heterostructure systems. Meanwhile, we found the coexistence of weak magnetism and insulating transport behavior in hydrogenated BM-LSMO(7/3) film distorted by tensile strain. Our results revealed that capped Pt electrodes can be considered to have a key role in the topotactic transformation of LSMO(7/3) film, which is beneficial to reconstruction of valence states of Mn ions, Mn–O interaction and concurrently enhanced magnetic properties at temperatures above > 400 K. Therefore, this work establishes a scalable route to engineer high-temperature FMIs in perovskite-based oxide films through hydrogen-induced topotactic transformation, expanding their potential for energy-efficient spintronic memory and logic devices.

Acknowledgement

This work was financially supported by the Guangdong Basic and Applied Basic Research Foundation (Grant

CPB Online In-Press

No. 2025A1515011057).

References

[1] Salahuddin S, Ni K and Datta S 2018 *Nat. Electron* **1** 442

[2] Puebla J, Kim J, Kondou K and Otani Y 2020 *Commun. Mater.* **1** 24

[3] Miao G X, Münzenberg M and Moodera J S 2011 *Rep. Prog. Phys* **74** 036501

[4] Li W, Zhu B, Zhu R, Wang Q, Lu P, Sun Y, Cafolla C, Qi Z, Chen A, Gao P, Wang H, He Q, Zhang K H L and MacManus-Driscoll J L 2020 *Adv. Funct. Mater.* **30** 2001984

[5] Li H B, Lou F, Wang Y, Zhang Y, Zhang Q, Wu D, Li Z, Wang M, Huang T, Lyu Y, Guo J, Chen T, Wu Y, Arenholz E, Lu N, Wang N, He Q, Gu L, Zhu J, Nan C W, Zhong X, Xiang H and Yu P 2019 *Adv. Sci.* **6** 1901432

[6] Hayashi N, Yamamoto T, Kageyama H, Nishi M, Watanabe Y, Kawakami T, Matsushita Y, Fujimori A and Takano M 2011 *Angew. Chem. Int. Ed. Engl.* **50** 12547

[7] Wang Y, He Q, Ming W, Du M H, Lu N, Cafolla C, Fujioka J, Zhang Q, Zhang D, Shen S, Lyu Y, N'Diaye A T, Arenholz E, Gu L, Nan C, Tokura Y, Okamoto S and Yu P 2020 *Phys. Rev. X* **10** 021030

[8] Zhang Q, Gao A, Meng F, Jin Q, Lin S, Wang X, Xiao D, Wang C, Jin K J, Su D, Guo E J and Gu L 2021 *Nat. Commun.* **12** 1853

[9] Meng D, Guo H, Cui Z, Ma C, Zhao J, Lu J, Xu H, Wang Z, Hu X, Fu Z, Peng R, Guo J, Zha X, Brown G J, Knize R and Lu Y 2018 *Proc. Natl. Acad. Sci. USA* **115** 2873

[10] Choi E M, Patnaik S, Weal E, Sahonta S L, Wang H, Bi Z, Xiong J, Blamire M G, Jia Q X and MacManus-Driscoll J L 2011 *Appl. Phys. Lett.* **98** 012509

[11] Wakabayashi Y K, Krockenberger Y, Tsujimoto N, Boykin T, Tsuneyuki S, Taniyasu Y and Yamamoto H 2019 *Nat. Commun.* **10** 535

[12] Zhou T, Gao F, Zhang Q, Chen Y, Hu X, He Y, Zhao Y, Li J, Li M, Qi S, Hu F, Sun J, Chen Y and Shen B 2025 *Nat. Commun.* **16** 3691

[13] Boschker H, Kautz J, Houwman E P, Siemons W, Blank D, Huijben M, Koster G, Vailionis A and Rijnders G 2012 *Phys. Rev. Lett.* **109** 157207

[14] Urushibara A, Moritomo Y, Arima T, Asamitsu A, Kido G and Tokura Y 1995 *Phys. Rev. B* **51** 14103

[15] Guo H, Dong S, Rack P D, Budai J D, Beekman C, Gai Z, Siemons W, Gonzalez C M, Timilsina R, Wong A T, Herklotz A, Snijders P C, Dagotto E and Ward T Z 2015 *Phys. Rev. Lett.* **114** 256801

[16] Liao Z, Li F, Gao P, Li L, Guo J, Pan X, Jin R, Plummer E W and Zhang J 2015 *Phys. Rev. B* **92** 125123

[17] Chen S, Zhou H, Ye X, Chen Z, Zhao J, Das S, Klewe C, Zhang L, Lupi E, Shafer P, Arenholz E, Jin D, Huang H, Lu Y, Li X, Wu M, Ke S, Xu H, Zeng X, Huang C, Martin L W and Chen L 2019 *Adv. Funct. Mater.* **29** 1907072

[18] Liao Z, Huijben M, Zhong Z, Gauquelin N, Macke S, Green R J, Van Aert S, Verbeeck J, Van Tendeloo G, Held K, Sawatzky G A, Koster G and Rijnders G 2016 *Nat. Mater.* **15** 425

[19] Coey J M D, Viret M and von Molnár S 1999 *Adv. Phys.* **48** 167

[20] Enriquez E, Chen A, Harrell Z, Lü X, Dowden P, Koskelo N, Janoschek M, Chen C and Jia Q 2016 *Appl. Phys. Lett.* **109** 141906

[21] Jang J, Jin Y, Nam Y S, Park H S, Kim J, Kang K T, So Y, Choi J, Choi Y, Shim J, Sriboriboon P, Lee D K, Go K J, Kim G Y, Hong S, Lee J H, Lee D, Han M G, Son J, Kim Y, Taniguchi H, Kang S, Lee J S, Tian H, Yang C H, Zhu Y, Cheong S W, Choi W S, Lee J and Choi S Y 2025 *Nat. Mater.* **24** 1228

[22] Kageyama H, Hayashi K, Maeda K, Attfield J P, Hiroi Z, Rondinelli J M and Poeppelmeier K R 2018 *Nat. Commun.* **9** 15

[23] Li D, Lee K, Wang B Y, Osada M, Crossley S, Lee H R, Cui Y, Hikita Y and Hwang H Y 2019 *Nature* **572** 624

[24] Lu Q, Huberman S, Zhang H, Song Q, Wang J, Vardar G, Hunt A, Waluyo I, Chen G and Yildiz B 2020 *Nat. Mater.* **19** 655

[25] Meng Z, Yan H, Qin P, Zhou X, Wang X, Chen H, Liu L and Liu Z 2023 *Adv. Funct. Mater.* **33** 2305225

[26] Ou J, Zhou H, Huang H, Rao F, Zeng X, Chen L, Shao R, Duan M and Huang C 2025 *Appl. Phys. Rev.* **12** 011412

[27] Yoon H, Choi M, Lim T W, Kwon H, Ihm K, Kim J K, Choi S Y and Son J 2016 *Nat. Mater.* **15** 1113

[28] Yang M, Liu Y, Chen G, Ou J, Peng J, Huang H, Zeng X, Leung C W and Huang C 2024 *Adv. Funct. Mater.* **34** 2408030

[29] Ni J Y, Wang P S, Lu J L and Xiang H J 2019 *Phys. Rev. Lett.* **122** 117601

[30] Huijben M, Martin L W, Chu Y H, Holcomb M B, Yu P, Rijnders G, Blank D H A and Ramesh R 2008 *Phys. Rev. B* **78** 094413

[31] Cao L, Petracic O, Zakalek P, Weber A, Rucker U, Schubert J, Koutsioubas A, Mattauch S and Bruckel T 2019 *Adv. Mater.* **31** 1806183

[32] Kubicek M, Cai Z, Ma W, Yildiz B, Hutter H and Fleig J 2013 *ACS Nano* **7** 3276

[33] Chen S, Guan C, Ke S, Zeng X, Huang C, Hu S, Yen F, Huang H, Lu Y and Chen L 2018 *ACS Appl. Mater. Interfaces* **10** 18029

[34] Wang Q, Gu Y, Zhu W, Han L, Pan F and Song C 2021 *Adv. Funct. Mater.* **31** 2106765

[35] Li J, Chen Y, Gong N, Huang X, Yang Z and Weng Y 2024 *Chin. Phys. B* **33** 017502

[36] Xu C, Jiang X, Zou Z, Xie Z, Zhang W and Feng M 2024 *Chin. Phys. B* **33** 127501

CPB Online Express